Explanation of Spin−Lattice Relaxation Rates of Spin Labels Obtained with Multifrequency Saturation Recovery EPR

Colin Mailer,[†] Robert D. Nielsen,[‡] and Bruce H. Robinson*[,‡]

Department of Radiology, University of Chicago, Chicago, Illinois, and Department of Chemistry, University of Washington, Seattle Washington 98195

Received: November 22, 2004; In Final Form: March 7, 2005

Electron paramagnetic resonance (EPR) pulsed saturation recovery (pSR) measurements of spin−lattice relaxation rates have been made on nitroxide-containing fatty acids embedded in lipid bilayers by Hyde and co-workers. The data have been collected for a number of spin-labeled fatty acids at several microwave spectrometer frequencies (from 2 to 35 GHz). We compare these spin−lattice relaxation rates to those predicted by the Redfield theory incorporating several mechanisms. The dominant relaxation mechanism at low spectrometer frequencies is the electron−nuclear dipolar (END) process, with spin rotation (SR), chemical shift anisotropy (CSA), and a generalized spin diffusion (GSD) mechanism all contributing. The use of a wide range of spectrometer frequencies makes clear that the dynamics cannot be modeled adequately by rigid-body isotropic rotational motion. The dynamics of rigid-body anisotropic rotational motion is sufficient to explain the experimental relaxation rates within the experimental error. More refined models of the motion could have been considered, and our analysis does not rule them out. However, the results demonstrate that measurements at only two suitably chosen spectrometer frequencies are sufficient to distinguish anisotropic from isotropic motion. The results presented demonstrate that the principal mechanisms responsible for anisotropically driven spin−lattice relaxation are well understood in the liquids regime.

I. Introduction

The recent publication of electron spin−lattice relaxation times (T_{1e}) of nitroxide spin-labeled stearic acid lipids (SASL) measured by the pulsed saturation recovery (pSR) technique at frequencies from 2.54 to 34.6 GHz by Hyde and co-workers is the motivation for this theoretical investigation[1] (referred to hereafter as HYSCRF).

These authors found the following: (i) The T_{1e} values of small water-soluble spin probes (common nitroxides Tempone and CTPO) increase linearly with the microwave frequency throughout the full range of available frequencies. (ii) The T_{1e} values of four commonly used lipid probes (nitroxide spin-labeled doxylstearic acid (SASL) and cholestane (CSL)) also increase with the frequency when incorporated in lipid bilayers. However, the relaxation times of the lipid-based probes have a nonlinear dependence on the microwave frequency in the higher frequency regime. (iii) The contribution of dissolved molecular oxygen to the relaxation rates is independent of the microwave frequency. (iv) The T_{1e} values of ^{15}N-containing labels are always somewhat longer than those of ^{14}N labels.

HYSCRF did not attempt to fit their multifrequency data to any model. We now present the details of a previously reported, but unpublished, theory that explains all of the features of spin−lattice relaxation noted above.[2] The data on isotropically moving spin labels (Tempol and CTPO) as well as the oxygen-collision relaxation results of HYSCRF are explained elsewhere [3,4] This paper focuses on providing an explanation of the relaxation rates of the lipid probes.

The prediction of relaxation rates requires that a dynamical process modulates the spin Hamiltonian. The effects of dynamics are included in the Redfield relaxation theory through spectral density functions that describe the fluctuations of the lattice.[4] We considered only two very simple dynamic processes: isotropic and anisotropic rigid-body rotational reorientation. The analysis of the spin−lattice relaxation rates relies primarily on the electron−nuclear dipolar (END) coupling between the electron and the nitroxide's nitrogen nucleus on the spin label. In addition to the END mechanism, we considered other mechanisms that contribute to the total spin−lattice relaxation of the electron.[3] (i) The chemical shift anisotropy (CSA) mechanism: the relaxation rates predicted from this mechanism are small relative to the END mechanism for processes in the dynamic and frequency ranges considered here, except at high microwave frequencies. At high microwave frequencies, both CSA and END rates are small, however. (ii) The spin-rotation (SR) mechanism: this mechanism is important for short correlation times, especially at high microwave frequencies. (iii) The generalized spin-diffusion mechanism (GSD): this semiempirical mechanism contributes at all frequencies and becomes important at the higher spectrometer frequencies where the other mechanisms drop out. It is a very general mechanism, with a weak power-law dependence upon the correlation time and the spectrometer frequency.[3] Recently, others[5] have demonstrated that the rotation of methyl groups on nitroxides may account for a portion of this mechanism. The general insensitivity of the GSD mechanism to correlation time allows for the rate to be replaced by a constant without much loss of accuracy.

Nitroxide spin probes are very useful in biological applications because they are sensitive to both molecular dynamics and to the composition of other paramagnetic species in the immediate environment of the spin probe. The direct determination of spin−lattice relaxation rates for nitroxides has led to

* Corresponding author. E-mail: robinson@chem.washington.edu.
[†] University of Chicago.
[‡] University of Washington.

10.1021/jp044671l CCC: $30.25
Published on Web 04/19/2005

new uses of these probes for biological problems.[6,7] However, wider use has been hindered by the lack of understanding of the relaxation mechanisms leading to the electron and nuclear spin−lattice relaxation rates of nitroxides. Our earlier work on isotropically moving spin labels[3,4] provided a largely satisfactory explanation of the effect of isotropic motion on the spin−lattice relaxation rate. The present paper is an extension of that work to anisotropic motion.

Spin-labeled fatty acid/membrane systems, typified by the SASL probes, have been a test bed for interpreting the effect of anisotropic motion on EPR spectra. Historically, SASLs were used to test the accuracy of CW simulation of anisotropic motion.[8] In HYSCRF, the membranes used were multilamellar dispersions of lipids (liposomes) containing 0.5 or 1 mol % of spin labels. The liposomes of DMPC (dimyristoylphosphatidylcholine) contained 5-, 12-, and 16-doxylstearic acid spin labels (5-, 12-, and 16-SASL). Their pSR spectra were acquired at 27 and 37 °C with the membranes in the fluid L_α phase.[9]

There has been an immense amount of EPR work on the anisotropic motion of spin labels in membranes from the 1970s on.[8,10−15] Virtually all of this investigation has been done with continuous-wave EPR (CWEPR) at X-band EPR frequencies (9.5 GHz). An important model for the motion of spin labels in membranes is the SRLS (slowly relaxing local structure) model of Freed an co-workers, wherein the nitroxide spin probe moves in a restricted local environment, which itself is reorienting on a longer time scale.[16,17] Fast motion arises from internal or local probe dynamics, whereas the slower motion describes the global tumbling of the macromolecule. Refinements of this model include the case when the global tumbling is the rigid limit, the microscopic-order macroscopic-disorder (MOMD) model. Another case is the fast internal motion (FIM) model, wherein the internal motion is so rapid that it leads to partial averaging of the magnetic tensors. Recently, a combined 250 and 9 GHz ESR study was performed on membrane vesicles composed of pure lipid (DPPC) and DPPC/cholesterol in a 1:1 molar ratio using the end-chain-labeled lipid, 16-PC.[18,19] Simultaneous fitting of both low and high-frequency CW EPR spectra was required to remove ambiguities among all of the various dynamic, ordering, and geometric factors that characterize the complex dynamics in these lipid systems. This multi-frequency study thus permitted the separation of both internal and global lipid motion.

There have been a number of attempts to compare the motion of lipids measured by NMR with those studied by CW EPR.[20,21] NMR measurements are made on deuterium-labeled lipids. The NMR spectra in the study of Kothe and co-workers were simulated using a line-shape model that incorporated chain-rotational isomerism as well as restricted anisotropic motion of the lipid molecules as a whole.[20] The simulation was valid in all of the motional regimes of conventional CW EPR spectroscopy as well. The simulation parameters yielded a consistent description for the chain order and dynamics for all of the label positions. The correlation times and order parameters for the overall motion were the same at all of the positions down the chain. These measures of overall reorientation had very similar values when determined by CW EPR and NMR. Such work gives confidence that a uniform motional model could be devised to cover a wide frequency range of motion.

The simulation of CW line shapes uses only those terms of the Hamiltonian (called the secular and pseudosecular terms) that are stationary at the microwave frequency, that is, in the rotating frame.[22a] The secular and pseudosecular terms do not contribute to the spin−lattice relaxation of the electron. Therefore, an explanation of spin−lattice relaxation requires other terms from a more complete Hamiltonian (the nonsecular terms). At the present time, only the Redfield theory is able to use the nonsecular terms to compute spin−lattice relaxation rates. The CW simulation techniques, which have been successful for anisotropic motion, are complementary to the work described herein but do not provide a methodology for spin−lattice rate calculations.

This paper shows that the microwave-frequency dependence of experimental spin−lattice relaxation rates measured by time-domain techniques is explained by a set of well-defined mechanisms with a very simple dynamics process using the Redfield relaxation theory. Future work will include additional mechanisms and more sophisticated dynamics processes. However, because no theory has been demonstrated that is capable of describing the magnitude and the frequency dependence of the spin−lattice relaxation rates, it is our goal to keep the Hamiltonians and the dynamics as simple as possible but still explain the general features of the relaxation rates. This work should provide a basis for a detailed quantitative explanation of the electron spin−lattice relaxation rates (or times) in any nitroxide spin-label system because the pertinent mechanisms have been isolated. The assumption of anisotropic rigid-body dynamics simplifies the relation between the model of spin-label dynamics and the spin−lattice relaxation rate. The relaxation rates given here may be extended by using correlation functions that are obtained from more sophisticated models or even the "model free" approaches.[23,24]

II. Theory

The Redfield theory of spin relaxation begins with a perturbation Hamiltonian, H', that consists of the spin operators and a fluctuating lattice contribution, usually in a form that is bilinear in spin and lattice variables. The relaxation rates are then computed from this Hamiltonian using the following approximate relation:[4,22a,25]

$$R_{1e} = \int_{\tau=0}^{\infty} \mathrm{tr}\{[O_z, \overline{H'^x(0)][H'^x(\tau)}, O_z^{\dagger}]\}\, \mathrm{d}\tau \qquad (1)$$

The perturbation Hamiltonian, H', enters eq 1 in a rotating frame that is generated by the stationary Hamiltonian: $H'^x(\tau) = \mathrm{e}^{-\mathrm{i}H_o\tau}H'\mathrm{e}^{+\mathrm{i}H_o\tau}$. The stationary Hamiltonian is $H_o = \omega_e S_z + \omega_n I_z + \bar{a} I_z S_z$. S represents the Cartesian components of electron spin, and I denotes the spin of the nitrogen nucleus. The bar over the two Hamiltonians represents averaging of the lattice operators over a stochastic process that ensures that the spin variables evolve toward thermal equilibrium. $O_z \propto S_z$ is the operator associated with the electron spin−lattice relaxation and satisfies the requirement that $\mathrm{tr}\{O_z^{\dagger}O_z\} = 1$. Because O_z is also Hermitian, or self-adjoint, only real-valued relaxation rates are computed.[26] A Redfield relaxation rate expression more general than eq 1 will have other operators, containing nuclear operators as well, in place of one of the O_z operators. This definition of R_{1e}, given by eq 1, neglects electron−nuclear cross relaxation rates (i.e., the Overhauser effect) and also neglects the cross coupling of the END and CSA mechanisms because only the O_z operator is accounted for. A more complete description of R_{1e}, published elsewhere, showed that these cross relaxation contributions are very small corrections in the motional range of the experiments considered here.[4] A unique feature of eq 1 is that there is no dependence on the nuclear manifold, that is, the spin−lattice relaxation rate, unlike the spin−spin relaxation rate, is independent of the nuclear manifold quantum number. The reason for this has been developed in detail elsewhere.[3,4]

The Hamiltonian, H', in eq 1 is the sum of the Hamiltonians for each of the four mechanisms introduced in section I. The rates associated with each of the four mechanisms considered, at the level of approximation embodied in eq 1, add independently.

$$R_{1e} = R_{1e}^{END} + R_{1e}^{CSA} + R_{1e}^{SR} + R_{1e}^{GSD}$$

We now develop the equations for the rates due to each of the individual mechanisms.

END Mechanism. The END Hamiltonian is $H_{END} = S\cdot(A - \bar{a})\cdot I$. A is the tensor coupling electron and nuclear spins. The isotropic part has been removed because it will not lead to a lattice correlation function. The secular term $\bar{a}S_zI_z$ is contained in H_o. The A tensor and spin operators are defined with respect to the laboratory frame. It is convenient to write the spin operators in terms of spherical tensor operators. The transformation, U, converts the Cartesian spin variables labeled x, y, and z to their spherical counterparts labeled -1, 0, and 1. The tensor A is also rotated to the principal axis system (PAS) in which A is diagonal. A is denoted by A in the diagonal frame. The rotation of A from the laboratory frame to the principal axis system is written in terms of the rotation matrix, $R(\Omega)$, and is parametrized by the Euler angles, Ω.

$$H_{END} = S^\dagger\cdot U^\dagger UR(\Omega)^\dagger U^\dagger U(A - \bar{a})\, U^\dagger UR(\Omega)U^\dagger U\cdot I = \boldsymbol{S}^\dagger\cdot D^1(\Omega)^\dagger\{U(A - \bar{a})U^\dagger\}\, D^1(\Omega)\cdot\boldsymbol{I}$$

where

$$D^1(\Omega) = UR(\Omega)U^\dagger \quad \boldsymbol{S} = U\cdot S \quad \boldsymbol{I} = U\cdot I$$

$$\text{and } U = \frac{1}{\sqrt{2}}\begin{pmatrix} 1 & -i & 0 \\ 0 & 0 & \sqrt{2} \\ -1 & -i & 0 \end{pmatrix} \quad (2)$$

$D^1(\Omega)$ is the rank 1 Wigner rotational matrix (WRM). The Clebsh-Gordan series reduces the product of two WRM elements to a sum over single WRM elements of higher rank and is used to simplify the Ω dependence of H_{END}.[27] The τ dependence of $H_{END}^x(\tau)$ can be evaluated explicitly if S and I are both spin $^1/_2$ variables[4] to give

$$H_{END}^x(\tau) = \sum_{m,n=-1}^{1} (-1)^q \boldsymbol{S}_n\boldsymbol{I}_m \begin{pmatrix} 1 & 1 & 2 \\ m & n & -q \end{pmatrix} e^{-i(n\omega_e + m\omega_n)\tau} \cos(n\tau(\bar{a}/2))\cos(m\tau(\bar{a}/2)) \sum_{p=-2}^{2} \alpha_p D_{p,q}^2(\Omega(\tau))$$

where α_p are elements of the vector

$$\vec{\alpha}^\dagger = (\alpha_2\ \alpha_1\ \alpha_0\ \alpha_{-1}\ \alpha_{-2}) = \sqrt{5}\left(a_-\ 0\ \sqrt{\frac{2}{3}}(a_+ - a_{zz})\ 0\ a_-\right)$$

$$a_\pm = \frac{a_{yy} \pm a_{xx}}{2}$$

and $D_{p,q}^2(\Omega)$ are the matrix elements of the second-rank WRM (5 by 5 matrices).

For spin-1 nuclei, the time-dependent terms of $H_{END}^x(\tau)$ that contain $\bar{a}$ are more complicated. However, for the electron spin−lattice relaxation rate, the time dependence arising from either $\bar{a}$ or ω_n is negligible. The oscillating terms containing $\bar{a}$ and ω_n are slowly changing on the time-scale of the terms containing ω_e because ω_e is a much higher frequency than either $\bar{a}$ or ω_n and can therefore be ignored when computing the electron spin−lattice relaxation rates. For example, the lowest microwave frequency, $\omega_e/2\pi$, that is considered here is 2.53 GHz, and the ^{14}N $\omega_n/2\pi$ is 0.3 MHz. The value of $\bar{a}$ for 5-SASL is 43 MHz. (See Table 2.)

TABLE 1: Spin−Lattice Relaxation Rates Predicted from the Equation of Owenus et al.[5] for Methyl Diffusion and that of Robinson et al.[3] for Spin Diffusion

frequency (GHz)	2.54	3.45	9.2	18.5	34.6
R_{1e}^{GSD-A} (Mrad/s)	0.22	0.19	0.088	0.045	0.024
R_{1e}^{GSD-B} (Mrad/s)	0.20	0.18	0.13	0.098	0.078

The components of $H_{END}^x(\tau)$ are grouped together so that the relaxation rate is written in terms of matrix and vector multiplication. Defining the elements of the spin operators as

$$V_q(\tau) = \sum_{n=-1}^{1} (-1)^q \boldsymbol{S}_n\boldsymbol{I}_m \begin{pmatrix} 1 & 1 & 2 \\ m & n & -q \end{pmatrix} e^{-in\omega_e\tau}$$

where $m = q - n$, $H_{END}^x(\tau)$ can be written as

$$H_{END}^x(\tau) = \vec{\alpha}^\dagger\cdot D^2(\Omega(\tau))\cdot\vec{V}(\tau) \quad (3)$$

Substituting eq 3 into eq 1

$$R_{1e}^{END} = \int_{\tau=0}^{\infty} \mathrm{tr}\{[O_z, \vec{V}^\dagger(0)]\cdot\overline{D^{2\dagger}(\Omega(0))\cdot\vec{\alpha}\vec{\alpha}^\dagger\cdot D^2(\Omega(\tau))}\cdot [\vec{V}(\tau), O_z^\dagger]\}\, d\tau \quad (4)$$

The lattice equilibrium process, represented by the bar in the integrand of eq 4, is assumed to be anisotropic Brownian dynamics. The correlation functions of $D^2(\Omega)$ matrix elements are evaluated most easily in the PAS of the anisotropic diffusion tensor, which may differ by a fixed rotation from the PAS of A. $D^2(\Omega)$ is decomposed into two rotations: a rotation from the laboratory frame to the PAS of the diffusion tensor, $D^2(\Omega')$, followed by a rotation from the PAS of the diffusion tensor to the PAS of A, $D^2(\Omega_{D-A})$. In terms of WRMs

$$D^2(\Omega) = D^2(\Omega_{D-A})\cdot D^2(\Omega')$$

Equation 4 becomes

$$R_{1e}^{END} = \sum_{p,q,p',q'} W_{p',p} \int_{\tau=0}^{\infty} \mathrm{tr}\{[O_z, V_{q'}^\dagger(0)][V_q(\tau), O_z^\dagger]\}\cdot\overline{D^{2*}_{p',q'}(\Omega')\, D^2_{p,q}(\Omega'(\tau))}\, d\tau \quad (5)$$

where

$$W = D^{2\dagger}(\Omega_{D-A})\cdot(\vec{\alpha}\vec{\alpha}^\dagger)\cdot D^2(\Omega_{D-A})$$

The trace over the spin variables in eq 5 is evaluated from the commutation and trace properties of the spin operators that make up the individual elements of V_q. Because O_z represents a spin $^1/_2$ observable

$$O_z = \frac{\sqrt{2}}{\sqrt{2I+1}}\cdot S_z\cdot 1_I$$

where 1_I is the unit operator in the space of the nuclear spin.

$$\mathrm{tr}\{[O_z, \boldsymbol{S}_n^\dagger \boldsymbol{I}_m^\dagger][\boldsymbol{S}_{n'}\boldsymbol{I}_{m'}, O_z^\dagger]\} = \delta_{n,n'}\delta_{m,m'}\cdot n^2\,\frac{I(I+1)}{3}$$

Therefore

$$\mathrm{tr}\{[O_z, V_{q'}^{\dagger}(0)][V_q(\tau), O_z^{\dagger}]\} = \delta_{q,q'} \sum_{n+m=q} C_{m,n} e^{-in\omega_e\tau} \quad (6)$$

where

$$C_{m,n} = n^2 \frac{I(I+1)}{3} \begin{pmatrix} 1 & 1 & 2 \\ m & n & -(m+n) \end{pmatrix}^2$$

The rotational correlation functions

$$\overline{D^{2*}_{p',q'}(\Omega')\, D^{2}_{p,q}(\Omega'(\tau))}$$

in eq 5 remain to be evaluated. In the most general treatment of rotational Brownian motion, the angular momentum and Euler angles of the rigid body are coupled. The correlation functions have the general form[28]

$$\overline{D^{2}_{p',q'}{}^{*}(\Omega(\tau))\, D^{2}_{p,q}(\Omega(0))} = \delta_{q,q'} \cdot G_{p,p'}(\tau) \quad (7)$$

Using eqs 6 and 7, eq 5 becomes

$$R_{1e}^{\mathrm{END}} = \sum_{p,p',n,m} W_{p,p'} \cdot C_{m,n} \cdot J_{p,p'}(n\omega_e) =$$
$$\frac{I(I+1)}{3} \sum_{p,p'} W_{p,p'} \left\{ \frac{1}{5} + \frac{1}{10} + \frac{1}{30} \right\} (J_{p,p'}(\omega_e) + J_{p,p'}(-\omega_e)) =$$
$$\frac{2}{9} I(I+1) \sum_{p,p'} W_{p,p'} \cdot \mathscr{R}(J_{p,p'}(\omega_e)) \quad (8)$$

where

$$J_{p,p'}(n\omega_e) = \int_{\tau=0}^{\infty} G_{p,p'}(\tau) e^{-in\omega_e\tau}\, d\tau$$

The coefficients, $C_{m,n}$, which come from the trace over the matrix representations to the spin operators, only allow $n = \pm 1$ values and ensure that the spectral density functions are always evaluated at ω_e.

The general spectral density functions, $J_{p,p'}$, have been treated in the literature.[28,29] Considerable simplification occurs when inertial effects are neglected, leaving only Brownian motion of the Euler angles. The dynamics of rigid-body anisotropic motion require two rates at a minimum, a parallel and a perpendicular diffusion coefficient, $d_{\|}$ and $d_{\perp}$. The diffusion tensor in the PAS has the form

$$D = \begin{pmatrix} d_{xx} & 0 & 0 \\ 0 & d_{yy} & 0 \\ 0 & 0 & d_{zz} \end{pmatrix} = \begin{pmatrix} d_{\perp} & 0 & 0 \\ 0 & d_{\perp} & 0 \\ 0 & 0 & d_{\|} \end{pmatrix} = \frac{1}{6} \begin{pmatrix} \tau_{\perp}^{-1} & 0 & 0 \\ 0 & \tau_{\perp}^{-1} & 0 \\ 0 & 0 & \tau_{\|}^{-1} \end{pmatrix} \quad (9)$$

The dynamics described by $d_{\|}$ and $d_{\perp}$ is the Brownian motion of a spherical top, for which the correlation functions are[30]

$$\overline{D^{2}_{p',q'}{}^{*}(\Omega'(\tau))\, D^{2}_{p,q}(\Omega'(0))} = \frac{1}{5} \delta_{p,p'} \delta_{q,q'} e^{-\tau(6d_{\perp} + p^2(d_{\|} - d_{\perp}))} =$$
$$\frac{1}{5} \delta_{p,p'} \delta_{q,q'} e^{-(\tau/\varsigma_p)} \quad (10)$$

where the inverses of the individual correlation times are

$$\frac{1}{\varsigma_p} = 6d_{\perp} + p^2(d_{\|} - d_{\perp})$$

The spectral densities for eq 10 are

$$\mathscr{R}(J_{p,p'}(n\omega_e)) = \delta_{p,p'} \frac{1}{5} \frac{\varsigma_p}{1 + (n\omega_e\varsigma_p)^2} \quad (11)$$

so that eq 8 gives

$$R_{1e}^{\mathrm{END}} = \frac{2}{45} I(I+1) \sum_{p} W_{p,p} \frac{\varsigma_p}{1 + (\omega_e\varsigma_p)^2} \quad (12)$$

Equation 12 is the final form of the END spin−lattice relaxation rate used in section III.

The rate (eq 12) depends on the rotation matrix, $D^2(\Omega_{D-A})$, which connects the PAS of the diffusion and hyperfine tensors, through $W_{p,p}$ coefficient. The angular dependence of eq 12 can be written directly in terms of $R(\Omega_{D-A})$ by first writing $W_{p,p} = \mathrm{tr}\{W \cdot \Lambda_p\}$, where Λ_p is the pth projection matrix. Λ_p can be expressed in terms of the $j = 2$ representation of the angular moment operator, J_z, as[31]

$$\Lambda_p = \prod_{m \neq p} \frac{J_z - m_1}{p - m}$$

$$\mathrm{tr}\{W \cdot \Lambda_p\} = \mathrm{tr}\{\vec{\alpha}\vec{\alpha}^{\dagger} \cdot D^2(\Omega_{D-A}) \cdot \Lambda_p \cdot D^{2\dagger}(\Omega_{D-A})\}$$

The components of angular moment transform under rotation as a vector[27]

$$D^2(\Omega_{D-A}) \cdot J_z \cdot D^{2\dagger}(\Omega_{D-A}) = R_{3,1}(\Omega_{D-A}) \cdot J_x +$$
$$R_{3,2}(\Omega_{D-A}) \cdot J_y + R_{3,3}(\Omega_{D-A}) \cdot J_z$$

The rotation matrix elements depend on two angles. There is a major, azimuthal tilt angle that specifies the relative angle of the Z components. The minor tilt angle specifies the $X-Y$ direction of the tilt. If only a single tilt angle is considered in the direction of the Y axis then

$$R_{3,1} = 0,\ R_{3,2}(\Omega_{D-A}) = \sin(\theta) \qquad R_{3,3}(\Omega_{D-A}) = \cos(\theta).$$

The explicit form of the spin−lattice relaxation rate is

$$R_{1e}^{\mathrm{END}} = \frac{2}{9} I(I+1) \sum_{p} c_p \frac{\varsigma_p}{1 + (\omega_e\varsigma_p)^2} \quad (13)$$

where

$$c_{\pm 2} = \frac{1}{16}(a_{yy} - 2a_{xx} + a_{zz} + (a_{yy} - a_{zz})\cos(2\theta))^2$$

$$c_{\pm 1} = \frac{1}{4}(a_{yy} - a_{zz})^2 \sin^2(2\theta) \quad (14)$$

$$c_0 = \frac{1}{24}(a_{yy} - 2a_{xx} + a_{zz} - 3(a_{yy} - a_{zz})\cos(2\theta))^2$$

and

$$\sum_{p} c_p = \{(a_{xx} - \bar{a})^2 + (a_{yy} - \bar{a})^2 + (a_{zz} - \bar{a})^2\}$$

TABLE 2.

tensors (PAS)	*XX*	*YY*	*ZZ*
A (in Gauss)	6.3	5.9	32.0
G	2.0090	2.0060	2.0020
I (in amu − Å²)	1000	1000	1000

The isotropic case can be recovered from eqs 12 and 13 by setting $\varsigma_p = \tau_c$ and gives the standard result:[3,22a]

$$R_{1e}^{END} = \frac{2}{9} I(I+1)\{(a_{xx} - \bar{a})^2 + (a_{yy} - \bar{a})^2 + (a_{zz} - \bar{a})^2\} \frac{\tau_c}{1 + (\omega_e \tau_c)^2} \quad (15)$$

The maximum value of eq 15 as a function of correlation time occurs when $\omega_e\tau_c$ equals 1. At X band, for example, the maximum isotropic rate is 0.6 Mrad/s, using the known values of A for 5-SASL. (see Table 2).

The END mechanism applies not only to intramolecular electron−nitrogen dipolar interaction but also applies to electron−proton dipolar interactions within a nitroxide.

Chemical Shift Anisotropy Mechanism. The CSA Hamiltonian is $H_{CSA} = \beta_e H \cdot (G - \bar{g}) \cdot S$. G is the tensor coupling electron spin to the applied field and contains the spin−orbital contribution to the Hamiltonian. H is the external field, and β_e is the electronic Bohr magneton. We assume the field (H) is along the external $\hat{z}$ axis and has a magnitude that matches the Larmor frequency of the electron so that $\beta_e H = \omega_e/\bar{g} \cdot \hat{z}$. The CSA spin−lattice relaxation rate is treated in analogy to the END mechanism, with G replacing A. G represents G in its

$$\text{PAS where } G = \begin{pmatrix} g_{xx} & 0 & 0 \\ 0 & g_{yy} & 0 \\ 0 & 0 & g_{zz} \end{pmatrix}$$

The vector $\vec{\alpha}$ is replaced by

$$\vec{\gamma}^{\dagger} = \frac{\omega_e \sqrt{5}}{\bar{g}} \left(g_- \; 0 \; \sqrt{\frac{2}{3}}(g_+ - g_{zz}) \; 0 \; g_- \right) \text{ where } g_{\pm} = \frac{g_{yy} \pm g_{xx}}{2}$$

The CSA Hamiltonian in the rotating frame is

$$H_{CSA}^{x}(\tau) = \vec{\gamma}^{\dagger} \cdot D^2(\Omega(\tau)) \cdot \vec{V}^{CSA}(\tau) \quad (16)$$

$$V_q^{CSA} = (-1)^q S_q \cdot 1_I \begin{pmatrix} 1 & 1 & 2 \\ 0 & q & -q \end{pmatrix} e^{-i(q\omega_e)\tau}$$

As in the END treatment, the rotation $D^2(\Omega(\tau))$ is decomposed into a rotation from the laboratory frame to the PAS of the diffusion tensor, followed by a fixed rotation from the diffusion tensor to the PAS of the G tensor. $D^2(\Omega) = D^2(\Omega_{D-G}) \cdot D^2(\Omega')$

Equation 16 is substituted into eq 1 to give

$$R_{1e}^{CSA} = \frac{1}{5} \sum_{p,p'} W_{p,p'}^{CSA} \mathcal{R}(J_{p,p'}(\omega_e)) \quad (17)$$

where

$$W^{CSA} = D^{2\dagger}(\Omega_{D-G}) \cdot (\vec{\gamma}\vec{\gamma}^{\dagger}) \cdot D^2(\Omega_{D-G})$$

In the case of Brownian anisotropic motion with no inertial effects, the spectral density functions are given by eqs 10 and 11, so the CSA relaxation rate is

$$R_{1e}^{CSA} = \frac{1}{25} \sum_p W_{p,p}^{CSA} \frac{\varsigma_p}{1 + (\omega_e \varsigma_p)^2} \quad (18)$$

The rate (eq 18) can be rewritten in complete analogy to eq 13 with a dependence on a single tilt angle between the diffusion tensor and the G tensor.

The isotropic case of eq 18 is recovered by setting $\varsigma_p = \tau_c$ and gives the standard result[22a]

$$R_{1e}^{CSA} = \frac{1}{5} \omega_e \left\{ \left(\frac{g_{xx} - \bar{g}}{\bar{g}} \right)^2 + \left(\frac{g_{yy} - \bar{g}}{\bar{g}} \right)^2 + \left(\frac{g_{zz} - \bar{g}}{\bar{g}} \right)^2 \right\} \left(\frac{\omega_e \tau_c}{1 + (\omega_e \tau_c)^2} \right) \quad (19)$$

The maximium value of eq 19 as a function of correlation time, at a fixed spectrometer frequency, occurs when $\omega_e\tau_c$ equals 1. At X band, for example, the maximum isotropic rate is 0.03 Mrad/s, using the known values of G for 5-SASL (see Table 2). For a fixed correlation time, τ_c, the maximum rate, as a function of the spectrometer frequency, occurs when the spectrometer frequency goes to infinity and is

$$R_{1e}^{CSA-MAX} = \frac{1}{5\tau_c} \sum_{i=1}^{3} \left(\frac{g_{ii} - \bar{g}}{\bar{g}} \right)^2.$$

Therefore, at large spectrometer frequency the CSA is limited by the dynamics and at this point becomes competitive with (but not as large as) the SR mechanism, which is developed next. The CSA can never become a dominant mechanism in the large spectrometer frequency regime.

Spin−Rotation Mechanism. There has been limited discussion in the EPR literature on the application of anisotropic motion to the spin-rotation mechanism.[28,32,33] We briefly outline the application of anisotropic motion with spin rotation.

The spin−rotation Hamiltonian is $H_{SR} = -S \cdot (G - g_{free}) \cdot \omega$, where ω is the angular velocity of the nitroxide in the laboratory frame and g_{free} is the g value of the free electron. Both the angular velocity and the angular coordinates are stochastically modulated as a result of Brownian motion. The proper reference frame, in which to express the angular velocity correlation functions, is the PAS of the inertial tensor, which we assume is coincident with the diffusion tensor.[28] $R(\Omega')$ is the rotation from the laboratory frame to the PAS of the diffusion tensor. ω_I will denote the angular velocity in the PAS of the inertial/diffusion tensor, so that $\omega_I = R(\Omega') \cdot \omega$. As above, G in its PAS is denoted by G. $R(\Omega_{D-G})$ is the fixed rotation from the PAS of the diffusion tensor to the PAS of G.

$$H_{SR} = -S \cdot R^{-1}(\Omega') \cdot R^{-1}(\Omega_{D-G}) \cdot (G - g_{free}) \cdot R(\Omega_{D-G}) \cdot R(\Omega') \cdot \omega = -S \cdot R^{-1}(\Omega') \cdot R^{-1}(\Omega_{D-G}) \cdot (G - g_{free}) \cdot R(\Omega_{D-G}) \cdot \omega_I$$

Transforming into a spherical basis with eq 2 gives

$$H_{SR} = -S^{\dagger} \cdot D^{1\dagger}(\Omega') \cdot \boldsymbol{g} \cdot \omega_I = -\omega_I^{\dagger} \cdot \boldsymbol{g}^{\dagger} \cdot D^1(\Omega') \cdot S \quad (20)$$

where

$$\boldsymbol{g} = U \cdot R^{-1}(\Omega_{D-G}) \cdot (G - g_{free}) \cdot R(\Omega_{D-G})$$

The angular velocity is left in its Cartesian coordinates to facilitate the use of the known velocity correlation functions. As a result, the spherical-to-Cartesian transformation matrix, U, has been absorbed into the definition of $\boldsymbol{g}$, leaving $\boldsymbol{g}$ non-Hermitian. The overall Hamiltonian is self-adjoint, however.

Inserting the spin-rotation Hamiltonian into eq 1 gives the spin−lattice relaxation rate due to the spin-rotation mechanism

$$R_{1e}^{SR} = \int_{\tau=0}^{\infty} \mathrm{tr}\{[O_z, \boldsymbol{S}^{\dagger}]\overline{D^{1\dagger}(\Omega')\cdot\boldsymbol{g}\cdot(\omega_I\omega_I{}^{\dagger}(\tau))\cdot\boldsymbol{g}^{\dagger}\cdot D^1(\Omega'(\tau))} [\boldsymbol{S}(\tau), O_z{}^{\dagger}]\}\,\mathrm{d}\tau \quad (21)$$

The effects of Brownian dynamics are contained in the combined rotation and angular velocity correlation functions. The elements of the $\boldsymbol{g}$ tensor are time-independent. It is necessary to write the matrices out as individual elements to obtain the correlation functions explicitly.

$$R_{1e}^{SR} = \int_{\tau=0}^{\infty} \mathrm{tr}\{C^{\dagger}\overline{D^{1\dagger}(\Omega'(0))\boldsymbol{g}\cdot(\omega_I\omega_I{}^{\dagger}(\tau))\cdot\boldsymbol{g}^{\dagger}D^1(\Omega'(\tau))} C(\tau)\}\,\mathrm{d}\tau = \sum_{n,n',p,p',m,m'} \int_{\tau=0}^{\infty} \mathrm{tr}\{C_n^{\dagger}C_{n'}(\tau)\}$$
$$\overline{D^{1\dagger}(\Omega'(0))_{n,p}\boldsymbol{g}_{p,m}(\omega_I\omega_I{}^{\dagger}(\tau))_{m,m'}\boldsymbol{g}^{\dagger}{}_{m',p'}D^1(\Omega'(\tau))_{p',n'}}\,\mathrm{d}\tau = \sum_{n,n',p,p',m,m'} (\boldsymbol{g}^{*}_{p',m'}\boldsymbol{g}_{p,m}) \int_{\tau=0}^{\infty} \mathrm{tr}\{C_n^{\dagger}C_{n'}(\tau)\}\cdot$$
$$\overline{D^{1*}(\Omega'(0))_{p,n}D^1(\Omega'(\tau))_{p',n'}(\omega_I\omega_I{}^{\dagger}(\tau))_{m,m'}}\,\mathrm{d}\tau \quad (22)$$

where

$$C(\tau) = \begin{bmatrix} O_+\mathrm{e}^{\mathrm{i}\omega_e\tau} \\ 0 \\ O_-\mathrm{e}^{-\mathrm{i}\omega_e\tau} \end{bmatrix} = [\boldsymbol{S}(\tau), O_z{}^{\dagger}]$$

The commutation properties of the individual spin operators give

$$\mathrm{tr}\{C_n^{\dagger}C_{n'}(\tau)\} = \mathrm{e}^{\mathrm{i}n\omega_e\tau}\delta_{n,n'}(1-\delta_{n,0}) \quad (23)$$

The correlation functions for the most general case of anisotropic rigid-body motion were given by Hubbard and are of the form[32,34]

$$\overline{D^{1*}(\Omega'(0))_{p,n}D^1(\Omega'(\tau))_{p',n'}(\omega_I\omega_I{}^{\dagger}(\tau))_{m,m'}} = \delta_{n,n'}G_{p,p'}^{m,m'}(\tau) \quad (24)$$

Using eqs 23 and 24, eq 22 becomes

$$R_{1e}^{SR} = \sum_{p,p',m,m'} (\boldsymbol{g}^{*}_{p',m'}\boldsymbol{g}_{p,m})\{J_{p,p'}^{m,m'}(\omega_e) + J_{p,p'}^{m,m'}(-\omega_e)\} \quad (25)$$

Where

$$J_{p,p'}^{m,m'}(\omega_e) = \int_0^{\infty} G_{p,p'}^{m,m'}(\tau)\mathrm{e}^{-\mathrm{i}\omega_e\tau}\,\mathrm{d}\tau$$

Because we ignore inertial effects in our treatment of Brownian motion, $G_{p,p'}^{m,m'}(\tau)$ simplifies and is described by separate correlation functions for the angular coordinates and velocity.

$$\overline{D^{1*}(\Omega'(0))_{p,n}D^1(\Omega'(\tau))_{p',n'}(\omega_I\omega_I{}^{\dagger}(\tau))_{m,m'}} = \overline{D^{1*}(\Omega'(0))_{p,n}D^1(\Omega'(\tau))_{p',n}}\;\overline{(\omega_I\omega_I{}^{\dagger}(\tau))_{m,m'}}$$

The separate angle and velocity correlation functions were given by Hubbard under this approximation.[32] In the case of a spherical top where the transverse elements of the diffusion tensor are equal

$$\overline{D_{p,n}^{1*}(\Omega'(\tau))\,D_{p',n'}^{1}(\Omega'(0))} = \frac{1}{3}\delta_{p,p'}\delta_{n,n'}\mathrm{e}^{-\tau(2d_{\perp}+p^2(d_{\parallel}-d_{\perp}))} \quad (26)$$

This is the first-rank analogue of the correlation functions in eq 10.

The velocity correlation functions can be written as a diagonal 3 by 3 matrix for the case of a spherical top, where the transverse inertial components are equal, $I_{xx} = I_{yy} \neq I_{zz}$. The diffusion and inertial tensors are considered to be codiagonal.

$$\overline{\omega_I\omega_I{}^{\dagger}(\tau)} = \begin{pmatrix} \frac{k_BT}{I_{xx}}\mathrm{e}^{-B_x\tau}f_x(\tau) & 0 & 0 \\ 0 & \frac{k_BT}{I_{yy}}\mathrm{e}^{-B_y\tau}f_y(\tau) & 0 \\ 0 & 0 & \frac{k_BT}{I_{zz}}\mathrm{e}^{-B_z\tau}f_z(\tau) \end{pmatrix} \quad (27)$$

where

$$f_{m=x,y} = \mathrm{e}^{C}\mathrm{e}^{-C(B_z\tau+\mathrm{e}^{-B_z\tau})}, \quad f_{m=z} = 1, \quad \text{and } C = \frac{k_BT}{I_{zz}B_z^2}\left(\frac{I_{xx}-I_{zz}}{I_{xx}}\right)^2$$

In the case of isotropic motion, the factors f_k are all equal to unity.

The angular velocity drag terms, B_m, are connected to the orientation diffusion coefficients through the friction tensor. The general relations using the friction tensor, F, are $D = k_BTF^{-1}$ and $B = F\cdot I^{-1}$. The combined identity (the Hubbard relation) is

$$d_mB_m = \frac{k_BT}{I_{mm}}$$

where $m = \{x, y, z\}$.[30] It is convenient to define the correlation times associated with the diffusion coefficients as

$$\tau_m = \frac{1}{6d_m}$$

Using eqs 26 and 27, eq 24 becomes

$$G_{p,p'}^{m,m'}(\tau) = \frac{1}{3}\delta_{m,m'}\delta_{p,p'}\mathrm{e}^{-\tau(2d_{\perp}+p^2(d_{\parallel}-d_{\perp}))}\frac{k_BT}{I_{mm}}\mathrm{e}^{-B_m\tau}f_m(\tau) \quad (28)$$

$G_{p,p'}^{m,m'}(\tau)$ in eq 28 is diagonal in both the upper and lower indices, allowing for further simplification of eq 25.

$$R_{1e}^{SR} = \sum_{p,m}\frac{1}{9\tau_m}|\boldsymbol{g}_{p,m}|^2\,J_p^m(\omega_e) \text{ where } J_p^m(\omega_e\tau) = \frac{3}{d_m}\mathscr{R}(J_{p,p}^{m,m}(\omega_e)) \quad (29)$$

The combined spectral density functions in expanded form are

$$J_p^{m=x,y} = B_x e^C \sum_{n=0}^{\infty} \frac{(-C)^n}{n!} \frac{((2d_\perp + p^2(d_{||} - d_\perp)) + B_x + (C+n)B_z)}{(\omega_e)^2 + ((2d_\perp + p^2(d_{||} - d_\perp)) + B_x + (C+n)B_z)^2}$$

$$J_p^z = B_z \frac{((2d_\perp + p^2(d_{||} - d_\perp)) + B_z)}{(\omega_e)^2 + ((2d_\perp + p^2(d_{||} - d_\perp)) + B_z)^2}$$

The spectral density, J_p^z, is a standard Lorentzian. J_p^x and J_p^y are both composed of sums of Lorentzians with increasing widths. In the motional regime where $B_k \gg \omega_e$ and $B_k \gg d_\perp$, $d_{||}$, the spectral density functions are unity and

$$R_{1e}^{SR} = \sum_{p,m} \frac{1}{9\tau_m} |\boldsymbol{g}_{p,m}|^2 \quad (30)$$

The sum over p can be simplified to bring eq 30 into a form that is similar to eqs 13 and 14 for the END relaxation rate.

$$\sum_p |\boldsymbol{g}_{p,m}|^2 = \sum_{p,q,q'} (R^{-1}(\Omega_{D-G})\cdot(G - g_{free})\cdot R(\Omega_{D-G}))_{q,m} (R^{-1}(\Omega_{D-G})\cdot(G - g_{free})\cdot R(\Omega_{D-G}))_{q',m} U^*_{p,q} U_{p,q'} = (R^{-1}(\Omega_{D-G})\cdot(G - g_{free})^2 \cdot R(\Omega_{D-G}))_{m,m}$$

Equation 30 becomes

$$R_{1e}^{SR} = \sum_{p,m} \frac{1}{9\tau_m} |\boldsymbol{g}_{p,m}|^2 = \sum_m \frac{1}{9\tau_m} (R^{-1}(\Omega_{D-G})\cdot(G - g_{free})^2 \cdot R(\Omega_{D-G}))_{m,m}$$

If a single tilt angle between the PAS of the diffusion tensor and G tensor is assumed, as in the development of the END and CSA mechanisms

$$R_{1e}^{SR} = \sum_m \frac{c_m}{9\tau_m}$$

where

$$c_x = (g_{xx} - g_{free})^2$$

$$c_y = (g_{yy} - g_{free})^2 \cos^2(\theta) + (g_{zz} - g_{free})^2 \sin^2(\theta) \quad (31)$$

$$c_z = (g_{zz} - g_{free})^2 \cos^2(\theta) + (g_{yy} - g_{free})^2 \sin^2(\theta)$$

The spin-rotation relaxation rate reduces to the well-known isotropic values when τ_m equals τ_c and B_m equals $\bar{B}$. For isotropic motion, eq 29 simplifies to

$$R_{1e}^{SR} = \frac{1}{9\tau_c}\{(g_{xx} - g_{free})^2 + (g_{yy} - g_{free})^2 + (g_{zz} - g_{free})^2\} \frac{\tau_c\bar{B}(1/3 + \tau_c\bar{B})}{(\omega_e\tau_c)^2 + (1/3 + \tau_c\bar{B})^2} \quad (32)$$

When $\omega_e\tau_c$ equals 1 and $\tau_c\bar{B} \gg 1$, the spin-rotation rate can be compared to the END and CSA. At X band, for example, the isotropic rate is 0.37 Mrad/s using the known values of G for 5-SASL (see Table 2).

General Spin-Diffusion Mechanism. General spin diffusion is comprised of a set of electron−nuclear mechanisms. Spin-diffusion mechanisms are based on through-space dipolar interaction of the electron spin with either nitroxide or solvent protons or deuterons. This mechanism is distinguished from the END mechanism above by the following: (1) the way in which the dipolar interaction is stochastically modulated and (2) the number of participating nuclei. For example, the distance between the nuclear and electron spin may be modulated stochastically if the moiety containing the nuclear spin is physically diffusing relative to the molecular frame. Rotation of the methyl groups adjacent to the N−O bond of the nitroxide modulates the methyl proton−electron distance. The methyl rotation is stochastic and is an example of diffusion. Unlike the END mechanism above, the distance between the electron and the nucleus is modulated, as opposed to the relative angle between the dipoles in END relaxation. The relaxation rate due to methyl rotation that has been suggested is[5]

$$R_{1e}^{GSD-A} = A\left(\frac{\omega_e\tau_{therm}}{1 + (\omega_e\tau_{therm})^2}\right) \quad (33)$$

where

$$A = \frac{2.8 \times 10^{16}}{2\pi(9.2 \times 10^9)} = 0.484 \text{ Mrad/s}$$

The effective diffusion time, τ_{therm}, is taken to be the thermally induced rotational reorientation time for the methyl groups, which is given by an approximate Arrhenius dependence

$$\tau_{therm} = \tau_c^o e^{(E_a/RT)} \text{ and } E_a = 9\text{kJ/mol} \equiv \text{or } \frac{E_a}{R} = 1100 \text{ K}$$
$$\tau_c^o = 2.5 \times 10^{-12} \text{ s}$$

Therefore, $\tau_{therm}(20\ ^\circ\text{C}) = 1.06 \times 10^{-10}$ s. If we compare τ_{therm} with the temperature dependence of the viscosity of water (modeled as an activated process with an activation energy of 2200 K·R)[35] and consider viscosity changes to be due to the effect of temperature on the solvent (water), we find that the effective diffusion time, τ_{therm}, will scale nearly as the rotational correlation time of the solvent to the $-1/2$ power. As a result, in the slow motion limit, $\omega_e\tau_{therm} \gg 1$, R_{1e}^{GSD-A} will depend on the rotational correlation time to the $-1/2$ power and will depend on the spectrometer frequency, ω_e, to the -1 power.

A more general spin-diffusion process involves the translational diffusion of proton-containing solvent molecules and has been treated by Torrey and others.[36,37] The translational diffusion of solvent in the vicinity of the nitroxide modulates the electron−solvent proton distance. The translational diffusion interaction scales with the inverse square root power of the translational correlation time, for Gaussian random flights. Simultaneously with this physical diffusion, however, there is diffusion of the solvent nuclear polarization in the network of the surrounding solvent protons by nuclear dipole−dipole "flip-flops". The proton−proton spin flip-flop transition rate occurs on a 10-ps time scale for water at room temperature.[22b] The nuclear polarization of the solvent protons can diffuse in and out of the vicinity of the electron spin by proton−proton interactions so that the solvent acts a bath of nuclear-spin polarization. The diffusion of nuclear polarization in the nuclear-spin system can modify the expression for relaxation by physical translational diffusion so that the resulting power-law dependence on correlation time of the total rate is not the inverse

square root dependence but is weaker. The form of the relaxation rate for this spin-diffusion mechanism,[3] which adapts deGennes theory of spin-diffusion to the relaxation of the electron, is[38]

$$R_{1e}^{SD-B} = R_{1e,max}^{SD}\left(\frac{2w_x\tau_d}{1+(\omega_e\tau_d)^{3/2}}\right)^{1/4} \qquad (34)$$

Here τ_d is the relative solvent−nitroxide translational diffusion time. The value of $R_{1e,max}^{SD} = 0.15$ Mrad/s has been measured at X band, and the reference frequency in the numerator is the X-band frequency $w_x = 2\pi(9.3\ \text{GHz})$.[3] At X band and when $\omega_e\tau_d$ equals 1, the spin diffusion rate is 0.15 Mrad/s. The expression (eq 34) suggests that in the slow motion limit, $\omega_e\tau_d \gg 1$, the relaxation rate should be proportional to the spectrometer frequency to the $-3/8$ power. Table 1 compares the GSD rates given by eqs 33 and 34 at the five frequencies of interest for 27 °C and $\tau_d = 2.5 \times 10^{-10}$ s. Table 1 shows that eqs 33 and 34 are quite similar at lower frequencies, but differ by a factor of 3 at the highest frequency.

Summary of Theory. The END and CSA mechanisms have the strongest dependence on the spectrometer frequency of the four mechanisms. The END relaxation rate is comprised of spectral densities of the form $\tau/(1 + \omega_e^2\tau^2)$, whereas CSA is proportional to terms with the form $\omega_e^2\tau/(1 + \omega_e^2\tau^2)$. In the fast motion limit, $\omega_e\tau \ll 1$, the END mechanism is independent of ω_e, whereas CSA scales as $\omega_e^2\tau$. In the slow motion limit, $\omega_e\tau \gg 1$, the END mechanism scales as $1/\omega_e^2\tau$, whereas the CSA mechanism is independent of ω_e. The frequency dependence of the END and CSA relaxation rates are therefore reciprocal. The spin-rotation relaxation rate (eq 31) is independent of the spectrometer frequency, whereas the spin diffusion mechanism possesses a weak $-3/8$-power-law dependence on ω_e. The examples of isotropic relaxation rates with $\omega_e\tau_c = 1$, provided above, illustrate that the isotropic END relaxation rate is the dominant mechanism at X band. It is therefore expected that the END mechanism will account for the majority of the spin−lattice relaxation-rate dependence on spectrometer frequency in the more complicated anisotropic case at X band and lower frequencies.

III. Results

The spin−lattice relaxation data from HYSCRF is fit with the four relaxation mechanisms given in section II using global analysis. The magnetic tensors for the doxyl spin probe are given in appendix IV of ref 10 and are shown in Table 2. The same magnetic tensors were used for each SASL position. The order of magnitude of the inertial tensor elements are estimated from the geometry of SASL and are given in Table 2. The spin-rotation rate (eq 29) reduces to eq 30 over the range of physically reasonable values for the inertial tensors so that the fitting function is insensitive to the inertial tensors. The inertial tensor elements were therefore fixed for the fitting.

Least-squares fitting is performed using a global analysis method to minimize the variance of the experimental data with the model

$$\sigma^2 = \sum_i w_i^2(R_{1e-exptl}^i - \hat{R}_{1e}{}^i)^2$$

We assume that the weights are $w_i \propto 1/(R_{1e-exptl}^i)$ and the weights are properly normalized, $\sum w_i^2$ equals 1. By weighting the data in this way, we minimized the relative errors. The weighted criterion is optimal when data spans a large range. When the theory is plotted on a logarithmic scale, the theory points appear as uniformly fitting the data. This follows because the difference of the logs of the experimental and theoretical rates, when the deviation is small, is close to the weighted rates

$$\ln(R_{1e-exptl}^i) - \ln(\hat{R}_{1e}^i) \approx \frac{R_{1e-exptl}^i - \hat{R}_{1e}^i}{R_{1e-exptl}^i}.$$

The application of weighted global analysis techniques enabled us to impose constraints among the parameters common to different data sets.

The data are first fit to an isotropic model of motion to illustrate the inadequacy of the isotropic expressions to account for the microwave-frequency dependence of the experimental relaxation rates. Figure 1, left, shows the ^{14}N SASL data and isotropic fits. The spin−lattice relaxation rate is plotted against the isotropic correlation time, τ_c (see eqs 15, 19, and 32 above). The error bars are the 6% error on the experimental relaxation rates (see ref 39, for example). The isotropic correlation time is the only adjustable parameter in the fit and is floated independently for each SASL label position. Circles are 27 °C data and squares are 37 °C data. The theory lines are labeled Q, K, X, S, and L from bottom to top according to spectrometer frequency. The ^{15}N data is shown in Figure 1, right, and was fit simultaneously with the ^{14}N data. The values of τ_c for ^{15}N were constrained to be the same as the ^{14}N data at each label position and temperature. Table 3, first column, shows the best-fit correlation times. To show the consistency of ^{14}N and ^{15}N data sets, we also fit the two data sets independently of each other. The results for the independent fits are reported in the 3rd and 4th columns of Table 3, and show a relative deviation of 5%. In all cases, the correlation times found for the 37 °C data were smaller than those for the 27 °C for the same label position, and the correlation times were smaller for the spin label further down the n-SASL chain.

The anisotropic model has three adjustable parameters: the mean correlation time

$$\bar{\tau} = \sqrt[3]{\tau_{||}\tau_{\perp}^2}$$

the magnetic tensor-diffusion tensor tilt angle, θ, and the anisotropy, $R = \tau_{\perp}/\tau_{||}$ (see eqs 9, 14, and 31). Minor tilt angles of 0 and 90° were tried, and the results were so similar that no effort to optimize this parameter was attempted. The minor tilt angle was fixed at 0°. Figure 2, left and right, shows the best-fit of the ^{14}N and ^{15}N data to the anisotropic model, where a single tilt angle and anisotropy are used for both sets of data at all label positions. Circles are 27 °C data, and squares are 37 °C data. The spin−lattice relaxation rates are plotted against the correlation time, $\tau_{\perp}$, which is related to $\bar{\tau}$ by

$$\tau_{\perp} = \sqrt[3]{R}\,\bar{\tau}$$

The error bars are the 6% relative errors reported from the experiments. The mean correlation time, $\bar{\tau}$, is constrained to be the same for the ^{14}N and ^{15}N data at each labeling position. The best-fit mean correlation times are given in the 2nd column of Table 3. The optimum value of the tilt angle is $\theta = 13.0 \pm 0.6°$, and the optimal anisotropy is $R = 68 \pm 6$.

The correlation times, τ_c, for the isotropic model are about 2 to 3 times larger than the $\bar{\tau}$ values of the anisotropic model, and the $\tau_{\perp}$ values of the anisotropic model are 4 times larger than the $\bar{\tau}$ values of the anisotropic model. Therefore, the isotropic model is optimized by the values of the correlation

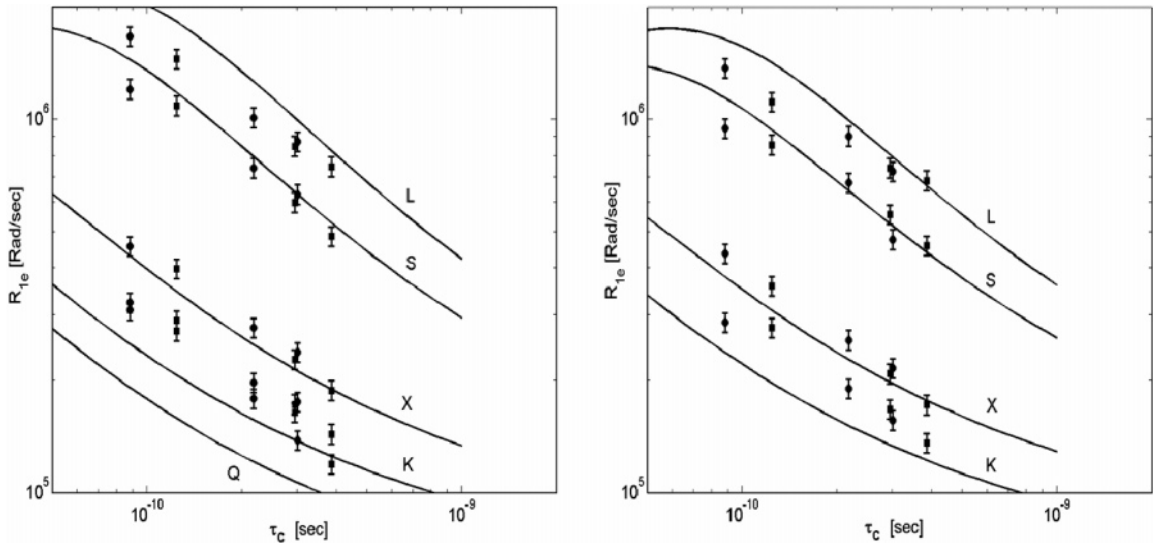

Figure 1. Isotropic simulation of multifrequency electron spin−lattice relaxation rates of n-SASL in DMPC liposomes. ^{14}N (left panel) and ^{15}N (right panel) isotopes are acquired at 27 (squares) and 37 °C (circles).[1] Spectrometer frequencies are L (2.54 GHz), S (3.45 GHz), X (9.2 GHz), K (18.5 GHz), and Q (34.6 GHz) bands. There is no data for the ^{15}N-sl at Q band (right panel). Error bars are the experimental uncertainty of 6%. Solid lines are the sum END, CSA, SR, and GSD relaxation mechanisms, plotted as a function of isotropic rotational correlation times, τ_c (see section II, text). Experimental rates are plotted with the isotropic rotational correlation time, τ_c, that best fits the solid lines assuming an identical τ_c for ^{14}N and ^{15}N data at equivalent temperatures and label positions (see Table 3, column 1). The A, G, and inertial tensors are given in Table 2.

TABLE 3. [a]

label position	τ_c [b]	$\bar{\tau}$ [c]	τ_c 14N-sl	τ_c 15N-sl	$\bar{\tau}$ 14N-sl	$\bar{\tau}$ 15N-sl
5-slDSL, 27 °C	0.39	0.22	0.40	0.36	0.22	0.21
12-slDSL, 27 °C	0.29	0.13	0.30	0.28	0.13	0.13
16-slDSL, 27 °C	0.12	0.038	0.12	0.13	0.037	0.040
5-slDSL, 37 °C	0.30	0.14	0.29	0.31	0.13	0.15
12-slDSL, 37 °C	0.22	0.084	0.23	0.21	0.087	0.081
16-slDSL, 37 °C	0.089	0.029	0.083	0.094	0.028	0.030

[a] All correlation times are in nanoseconds. Errors on all correlation times do not exceed 10%. [b] Isotropic correlation time. [c] $\bar{\tau} = \sqrt[3]{\tau_\perp^2 \tau_{||}}$

times, τ_c, that are midway between the $\bar{\tau}$ and $\tau_\perp$ values for the anisotropic model.

Figure 3 is a scatter plot of all of the experimental spin−lattice relaxation data (^{14}N and ^{15}N) plotted against the best-fit theory that locked the fitting parameters to be the same for ^{14}N and ^{15}N at each label position and temperature. Figure 3, left, is the scatter plot for the isotropic model, and Figure 3, right, is the anisotropic model. The average relative error for the isotropic fit is 18%. The average relative error for the anisotropic fit is 7%. The error on the experimental data points is 6%.[39] Therefore, the agreement of the anisotropic fit with the experimental data is nearly within the experimental accuracy. The improvement of fit to the 56 data points for the anisotropic model is at the cost of two more parameters than the comparable isotropic model. The χ_R^2 (reduced chi square) for the isotropic model is 9.0, as opposed to 1.4 for the anisotropic model. This represents a 6-fold improvement in χ_R^2 upon going from a model with six independent, adjustable parameters to one with eight parameters.

The constraints linking the correlation times, tilt angle, and anisotropy of the ^{14}N and ^{15}N data are removed to test whether the anisotropy model can better fit the data with additional degrees of freedom. Although separate tilt angles and anisotropies are not physically expected for the two different isotopes, the fitting illustrates whether the ^{14}N and ^{15}N data sets are consistent, and whether an improved fit, even if it is pathological, can be found. The 5th and 6th columns of Table 3 display the best-fit $\bar{\tau}$ values for the ^{14}N and^{15}N data when fit with separate correlation times. The tilt angle and anisotropy were identical within error to the case where a common $\bar{\tau}$ was used. The relative deviation of the two sets of $\bar{\tau}$ values obtained from the ^{14}N and ^{15}N data is 4% (see the fifth and sixth columns of Table 3), and the mean of the relative deviations is 0.15%. The average fitting error remained at 7%. Therefore, unlocking the correlation times for ^{14}N and ^{15}N data does not lead to improvement of the fit.

A further test is to allow for a different tilt angle and anisotropy for the ^{14}N and ^{15}N data, as well as different correlation times. The second and third columns of Table 4 contain the results for the separate fits of ^{14}N and ^{15}N data. The average fitting error is 6%, which is only a minor improvement of the average fitting error of 7% for locked data sets. The ^{14}N and ^{15}N data sets are optimized by different tilt angles and anisotropies. The ^{14}N correlation times (Table 4, second column) did not significantly change. The change in tilt angle and anisotropy represents a tradeoff between these two variables by decreasing the value of θ and increasing the value of R. The value of θ is identical within error to the locked case. The value of R nearly overlaps with the value found with ^{14}N and ^{15}N data sets locked. In contrast, the ^{15}N correlation times increased by 0.02 ns on average. The tilt angle and anisotropy also showed tradeoff by increasing the value of θ and decreasing the value of R.

IV. Discussion

The results from section III demonstrate that an anisotropic model of SASL dynamics is necessary for a proper description of the microwave-frequency dependence of the spin−lattice relaxation rates. Previous work on isotropically moving small nitroxides has shown that the four relaxation mechanisms used here are sufficient to predict the isotropic spin−lattice relaxation rates quantitatively at X band.[3] Figures 1 and 3, left, show that the isotropic theory of relaxation rates does not fit the SASL data. In contrast, the generalization of the four mechanisms to anisotropic motion (detailed in section II) allows for a good fit to the SASL data. The agreement with the data is achieved with the anisotropic model by the addition of only two new adjustable

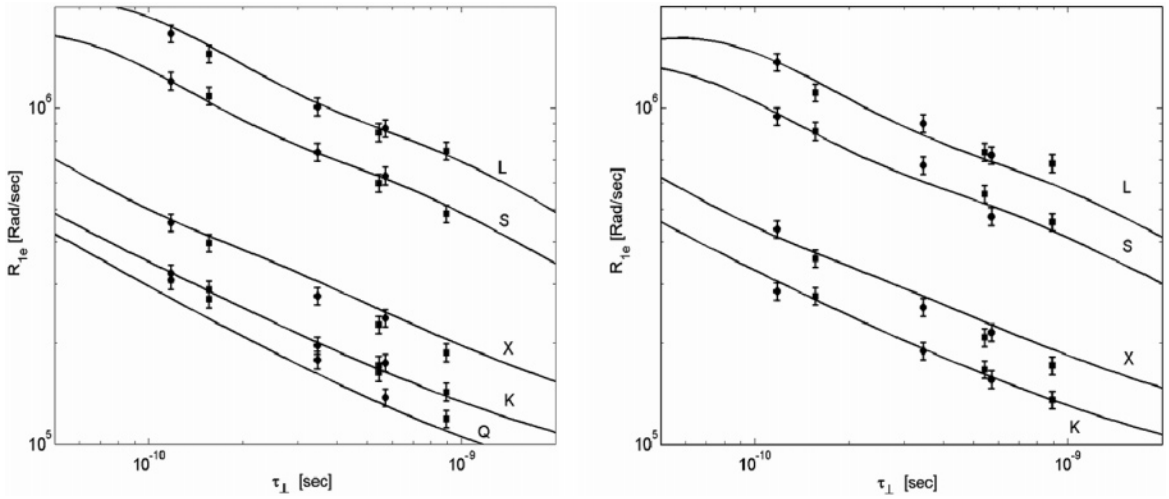

Figure 2. Anisotropic simulation of multifrequency electron spin−lattice relaxation rates of n-SASL in DMPC liposomes. ^{14}N (left panel) and ^{15}N (right panel) isotopes are acquired at 27 (squares) and 37 °C (circles).[1] Spectrometer frequencies are L (2.54 GHz), S (3.45 GHz), X (9.2 GHz), K (18.5 GHz), and Q (34.6 GHz) bands. There is no data for the ^{15}N-sl at Q band (right panel). Error bars are the experimental uncertainty of 6%. Solid lines are the sum END, CSA, pSR, and GSD relaxation mechanisms plotted as a function of the transverse anisotropic rotational correlation time, $\tau_\perp$. The anisotropy is $R = \tau_\perp/\tau_\parallel = 68$, and the tilt angle between the magnetic and diffusion tensors is $\theta = 13°$ (see text). Experimental rates are plotted with the $\tau_\perp$ that best fits the solid lines assuming an identical $\tau_\perp$ for ^{14}N and ^{15}N data at equivalent temperatures and label positions (see Table 3, column 2, $\tau_\perp = \sqrt[3]{R}\cdot\bar{\tau}$). The A, G, and inertial tensors are given in Table 2. See Table 4 for more details of the dependence of the data on correlation times.

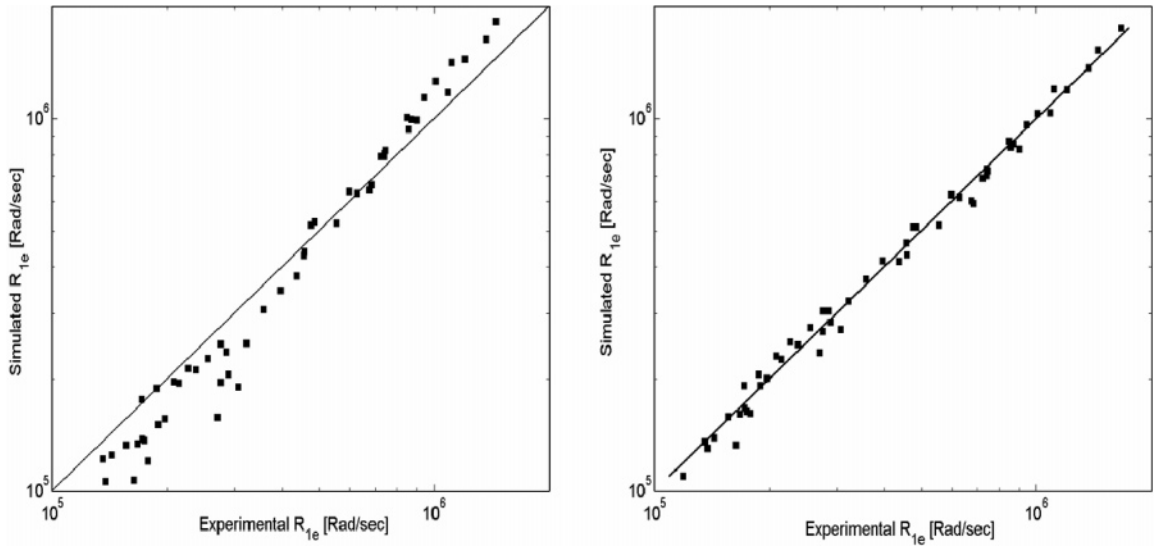

Figure 3. Scatter plot of the experimental spin−lattice relaxation rates and the simulated spin−lattice relaxation rates for the isotropic model (left panel, see Figure 1) and the anisotropic model (right panel, see Figure 2). Experimental values are plotted on the abscissa. The solid line on each figure represents perfect correlation between the experiment and the simulation. The average relative average error for the isotropic fit is 18%. The average relative error for the anisotropic fit is 7%.

TABLE 4. [a]

label losition	$\bar{\tau}$ N14/15 locked	$\tau_\perp$ N14/15 locked	$\bar{\tau}$ ^{14}N	$\bar{\tau}$ ^{15}N
5-slDSL, 27 °C	0.22	0.90	0.22	0.23
12-slDSL, 27 °C	0.13	0.53	0.12	0.16
16-slDSL, 27 °C	0.038	0.16	0.034	0.048
5-slDSL, 37 °C	0.14	0.57	0.12	0.18
12-slDSL, 37 °C	0.084	0.34	0.081	0.098
16-slDSL, 37 °C	0.029	0.12	0.026	0.035
ratio	68(6)		85(9)	46(5)
tilt angle	13.0(6)°		12.3(7)°	15(1)°

[a] All correlation times are in nanoseconds. Errors on all correlation times do not exceed 10%.

parameters: the tilt angle between the magnetic and the diffusion tensors and the anisotropy of the diffusion. The decomposition of the relaxation rate into the four mechanisms, which is detailed in section II, using the best-fit parameters, illustrates how the frequency dependence of the spin−lattice relaxation rate arises.

The END relaxation mechanism is the primary mechanism responsible for a microwave-frequency dependence of the relaxation rates for the range of data analyzed here. Table 5A and B show the percentage contributions of the four mechanisms to the total relaxation rate, for the optimal tilt angle and anisotropy (see section III Figure 2) at two different values of $\tau_\perp$, which bracket the data. The CSA mechanism only enters in the high-frequency regime, where it contributes 20% to the total rate at most. At the higher spectrometer frequencies, the frequency-insensitive SR and GSD mechanisms dominate. Improved agreement of the anisotropic model over the isotropic model with the experimental data is achieved because the anisotropic expression for the END rate (eq 13) spreads the END

TABLE 5

	A: $\tau_\perp = 1 \times 10^{-10}$ s				
ν	34.6[a]	18.5	9.2	3.45	2.54
$\%R_1^{END}$	12.3[b]	25.7	46.6	79.0	85.3
$\%R_1^{CSA}$	13.2	6.0	2.1	0.4	0.2
$\%R_1^{SR}$	35.7	31.2	21.7	8.0	5.5
$\%R_1^{GSD}$	38.8	37.1	29.6	12.6	9.0
R_1^{total}	0.26[c]	0.34	0.51	1.42	2.06
	B: $\tau_\perp = 1 \times 10^{-9}$ s				
ν	34.6[a]	18.5	9.2	3.45	2.54
$\%R_1^{END}$	3.9[b]	10.4	27.0	62.2	71.2
$\%R_1^{CSA}$	8.7	6.3	3.3	0.6	0.4
$\%R_1^{SR}$	12.3	9.6	6.4	2.5	1.7
$\%R_1^{GSD}$	75.1	73.7	63.3	34.7	26.7
R_1^{total}	0.10[c]	0.13	0.20	0.52	0.75

[a] Microwave frequency in GHz. [b] All rates that contribute to the total are expressed as a percent of the total; for example, $\%R_1^{END} = 100\frac{R_1^{END}}{R_1^{Total}}$ for ^{14}N SASL at 27 °C. [c] Total relaxation rate in Mrad/s.

amplitude over several spectral density functions, as opposed to the single spectral density in the isotropic expression (eq 15). The spread of spectral density functions leads to a broadening of the domain of correlation times over which the END rate contributes.

The small tilt angle and the range of values of the correlation times found in this study can be compared with the findings of Lange and co-workers, who simulated the CW EPR spectra of labeled DMPC in oriented bilayers with a detailed model of anisotropic motion. Their study was of a spin-labeled myristate chain attached to the glycerol backbone of a DMPC lipid, rather than the free stearic acid incorporated in a lipid (analyzed here), so differences are expected. Lange and co-workers reported that in the fluid, L_α, phase of DMPC there is no net tilt of the lipid chains.[21] They also found that lipid chains rotate at an intermediate rate about their long axis in the range of 1−6 ns, and the reorientation of the chain axis is in the range from 13 to 60 ns. Additionally, they report a mode of motion consisting of rapid trans-gauche isomerization (at the C-6 position), characterized by a jump time $\tau_J \leq 0.2$ ns. Because the isomerization is a local phenomenon, motion on a similar time scale is expected in the free stearic acid chain of SASL. Freed and co-workers also reported correlation times that are intermediate between the fastest and longest times of Lange et al. for similar systems and attribute part of the motion to local modes as well.[18,19] The slowest correlation times found in this study, $\tau_\perp$, are comparable to the trans-gauche isomerization correlation times, which are 5−10 times faster than the axial rotation times reported by Lange et al. The faster set of correlation times, $\tau_{||}$, reported here, which are in the 10^{-11}−10^{-10} s range, may correspond to processes so fast that they are not directly observable by CW EPR spectroscopy. Rapid motion of this sort could explain why CW EPR reports no tilt angle in the fluid, L_α, phase, whereas we estimate a 13° tilt angle. Rapid fluctuations around the lipid chain axis would effectively generate an averaging of the tensor elements used in the CW EPR simulations and would rotate the averaged tensor elements to be more collinear with the lipid chain axis. This line of reasoning becomes even more plausible when one recalls that the trans-gauche isomerization is a jumping between two structures that differed by a 25−30° tilt angle in the gel phase. The jump times are bracketed by the two sets of correlation times reported here, and may well be averaged values of these times with dynamically averaged tilt angles and magnetic tensor elements.

As noted above, the terms in the Hamiltonian needed to simulate the spin−lattice relaxation rates are different from those used to simulate the CW EPR spectra. Therefore, in systems with a wide dynamic range of motional processes, such as lipids, it is not surprising that the different measurements would be sensitive to different motional processes and time scales for those processes. The information obtained from the spin−lattice relaxation rates must be considered to be complementary to that acquired from the CW EPR spectra. Therefore, it is not necessary that the motional rates seen in the two techniques be the same.

The average error of anisotropic fit given in section III is nearly within the experimental error of the relaxation rates. Unlocking the correlation time, tilt angle, and anisotropy between ^{14}N and ^{15}N data sets does not lead to significant improvement in the quality of the fit or significantly affect the ^{14}N optimized fitting parameters (see Table 4 and description). The ^{15}N data-set parameters did tradeoff of each other when unlocked from the ^{14}N set so that the optimized parameters were different between the ^{14}N and ^{15}N data sets. The quality of the final fit was not improved significantly over the locked case, however. In summary, the ^{14}N and ^{15}N data sets give consistent fit parameters independently.

The tilt angle and anisotropy can also be fit independently for each labeling position, but this does not lead to significant improvement of the fitting error (data not shown). Allowing a second (minor) tilt angle (see eq 12) does not lead to significant improvement of the fit either (data not shown). Therefore, further improvement of the quality of fit must involve changing the underlying model. We discuss several possibilities for improving the anisotropic model to improve the fit. When a greater library of multifrequency time-domain data becomes available, we anticipate that more detailed models will become necessary.

One possibility for fine-tuning the anisotropic relaxation rates is to revisit the relaxation mechanisms. A proton END mechanism could be potentially important for applications to general nitroxides. The proton END expression is completely analogous to the electron−nitrogen dipolar mechanism in section II and has the same spectral density functions. The magnitude of the coefficients, c_p, that make up the mixture of spectral density functions in eq 13 is the sole difference between the nitrogen and proton END rates. The proton END contribution to the relaxation should be dominated by the doxyl ring and methyl protons in the case of SASL, and we estimate the contribution of proton END to be 1 order of magnitude smaller than the nitrogen END rate, in the present case.

Another possible contribution to the relaxation rates arises from the cross correlation of the rates, mentioned in section II. Cross correlation terms, developed elsewhere,[4] are significant in the fast motion limit of dynamics $\omega_o\tau \ll 1$, wherein they can reduce the spin−lattice relaxation rate by approximately 2-fold for isotropic motion.[4] However, the correlation times and spectrometer frequencies appropriate to the SASL data are in the regime $\omega_o\tau \gtrsim 1$. Lower frequency and/or faster motion data may necessitate the inclusion of END/CSA cross correlation and the inclusion of other observables, which cross-relax with the electron spin−lattice observable.

The generalized spin-diffusion relaxation rate presented in section II differs from the END, CSA, and SR mechanisms because the relaxation expression is not known completely from first principles. There is no strong consensus in the literature

as to the exact form of this "floor" mechanism. The experimental data of HSCRF, as well as previous work demonstrate that there is a need for a mechanism that has a weak frequency dependence and a weak correlation-time dependence.[5,40,41] For example, the data used here show that if a model function were chosen that had no correlation time dependence but did have a frequency dependence, then the experimental rates would require such a model to have a $-^2/_3$ power dependence on spectrometer frequency. Two possible expressions were given in section II, with different origins. Both of these empirical models approximately meet these criteria.

The first approach, based on spin−lattice relaxation measurements at 9.2, 3.1, and 1.9 GHz,[5] introduced a diffusion model based on nitroxide methyl group rotation in which the rotational correlation time (eq 33) depended only on temperature. The second model is a generalized spin-diffusion expression that contains a $-^1/_8$ power dependence on correlation time (eq 34 above). The application of a spectral density function with such an unusually weak power-law-dependent mechanism was initiated in response to the experimental data of Fajer and Hyde on spin-labeled hemoglobin[40] as well as data of small nitroxides.[3] The difference in frequency and correlation-time dependence of the two proposed diffusion processes (eqs 33 and 34) is obscured over the correlation times appropriate to the SASL data. One advantage of the first model is that it does not require intermolecular interactions as suggested in the second model.[3] From Table 1, however, the first mechanism predicts rates that are too small to provide an adequate relaxation rate floor on the data at high frequencies and long correlation times. Although the relative differences between the relaxation rates of the two expressions (eqs 33 and 34) are small, we chose to use the second model for simulating the data. This model was calibrated with the isotropically moving nitroxides and used without any modification. Relaxation rates over an even wider class of nitroxides, frequencies, and temperatures will be necessary to fully establish the proper empirical form of this mechanism.

Finally, and perhaps most significantly, there is potential for improvement of the dynamics models. Rigid-body axial dynamics is the crudest model that incorporates anisotropic motion. There are clear routes for improving the underlying model. One method, which stays within the framework of section II, is to replace the correlation functions (eqs 10 and 26) with more general correlation functions. As a first step, correlation functions that describe nonaxial rigid-body anisotropic motion could be used.[32] Multiple time scales of motion can be included by using generalized spectral density functions constructed with a model-free approach.[23] It is possible that the trans-gauche isomerization model may provide a dynamics process that will give correlation functions similar to those required for more advanced treatments.

The stochastic Liouville equation (SLE) gives an alternative method for the simulation of anisotropic motion, which does not proceed through correlation functions and does not utilize the Redfield formulation.[42] The SLE is typically used to simulate the continuous-wave EPR line shape but is adaptable to time-domain simulation.[43] The SLE approach has been generalized to include multiple time-scale processes. For example, the MOMD and FIM models of Freed and co-workers have been successful for the simulation of complicated biological CW spectra that involve anisotropy and multiple time scales of the dynamical processes.[17,19] CW EPR is not sensitive to motions on the time scale of the spectrometer frequency (except for the line widths), and the effects of motion on the CW line shapes are maximal when the dynamics are on the order of the anisotropy of the tensors. In contrast, spin−lattice relaxation times are most sensitive to dynamic processes occurring on the order of the spectrometer frequency.

Spin−lattice relaxation relies on nonsecular terms in the Hamiltonians describing the interaction of the electron spin with nuclear spins, with the magnetic fields and with the angular momentum of the molecule. The Redfield theory relies on dynamics to generate fluctuations in these Hamiltonians. In contrast, the line shapes and CW spectra depend only on the stationary or secular (and pseudosecular) terms in the Hamiltonians. The nonsecular terms do not directly contribute to the Hamiltonian used to simulate CW line shapes. In CW EPR line-shape simulations, the underlying spin−spin and spin−lattice relaxation rates are not computed from first principles. After simulation, the origin of the rates are sometimes analyzed in terms of the underlying dynamics using the Redfield theory.[13,44,45] The Redfield theory has been quite successful in providing an understanding of how anisotropic dynamics affect spin−spin relaxation rates. Now spin−lattice relaxation rates are analyzed properly by mechanisms analogous to those used for spin−spin relaxation rates. Typically, the fundamental spin−lattice relaxation rate is included in time-domain simulations as a constant.[43] The resulting simulation of the time-domain spectrum then is done to take into account the details of the effects of the pulse sequences and distortions that alter the apparent relaxation rate from the underlying fundamental rate.

The challenge for detailed models is not only to obtain the proper CW line shape but also to simultaneously generate proper spectral density functions that explain the experimentally observed spin−lattice relaxation rates. The SLE method must be expanded to include Hamiltonians that are fluctuating in the rotating frame to be used to simulate time-domain spectra that encompass dynamics processes containing motion on many time scales. When this is accomplished, the SLE method will be a computational platform capable of simulating both relaxation rates and CW line shapes simultaneously for multi-time-scale dynamics processes.

V. Conclusions

Previous work on nitroxide spin−lattice relaxation in isotropic motional systems presented the four mechanisms considered here (END, CSA, SR, and GSD). That work showed that the mechanisms were adequate to explain the spin−lattice relaxation rates for both the electron and the nitrogen nucleus of nitroxide spin probes with motional processes ranging from 10 ps to 0.1 ms.[3] The work here has successfully extended this analysis to an anisotropic system by making the END, CSA, and SR mechanisms anisotropic. A very simple model of anisotropic rigid-body motion was used to develop the spectral density functions needed to analyze the spin−lattice relaxation rates. Despite the simplicity of the model, the agreement with the data was almost at the experimental error. The measurement of spin−lattice relaxation rates is complementary to CW EPR spectra because none of the Hamiltonians used to simulate spin−lattice relaxation rates are included in the CW EPR line-shape simulations used to model CW spectra. Therefore, although it is gratifying that the time scale of some of the dynamic processes determined from fitting the spin−lattice relaxation rates are quite similar to those obtained from simulating CW EPR line shapes, it is not surprising that other processes were found that are much faster than those used in line-shape simulations. More investigation is necessary to fully characterize the spin diffusion mechanism and to develop the necessary correlation functions that are appropriate for more detailed models of lipid dynamics.

However, the present work does demonstrate that the relaxation mechanisms are well understood, a multi-mechanism approach is necessary, and a first-principles calculation of relaxation rates can quantitatively fit the experimental data.

Acknowledgment. This work was supported by grants HL36235, HL50040, GM065944, and RR-12257 from the National Institutes of Health, UW Environmental Sciences Center grant P30-ESO7033 from NIEHS, and partial support from AFOSR.

References and Notes

(1) Hyde, J. S.; Yin, J. J.; Subczynski, W. K.; Camenisch, T. G.; Ratke, J. J.; Froncisz, W. *J. Phys. Chem. B* **2004**, *108*, 9524.
(2) Robinson, B. H.; Mailer, C.; Yin, J. J.; Hyde, J. *Anisotropic Motion in Spin-Labeled Lipids Studied by Multi-Frequency Saturation Recovery EPR*; 35th Rocky Mountain Conference, Denver, CO, 1993.
(3) Robinson, B. H.; Haas, D. A.; Mailer, C. *Science* **1994**, *263*, 490.
(4) Robinson, B. H.; Reese, A. W.; Gibbons, E.; Mailer, C. *J. Phys. Chem. B* **1999**, *103*, 5881.
(5) Owenius, R.; Terry, G. E.; Williams, M. J.; Eaton, S. S.; Eaton, G. R. *J. Phys. Chem. B* **2004**, *108*, 9475.
(6) Altenbach, C.; Froncisz, W.; Hyde, J.; Hubbell, W. L. *Biophys. J.* **1989**, *56*, 1183.
(7) Nielsen, R. D.; Canaan, S.; Gladden, J. A.; Gelb, M. H.; Mailer, C.; Robinson, B. H. *J. Magn. Reson.* **2004**, *169*, 129.
(8) Van, S. P.; Birrell, G. B.; Griffith, O. H. *J. Magn. Reson.* **1974**, *15*, 444.
(9) Kusumi, A.; Subczynski, W. K.; Hyde, J. S. *Proc. Natl. Acad. Sci. U.S.A.* **1982**, *79*, 1854.
(10) *Spin Labeling: Theory and Applications*; Berliner, L. J., Ed.; Academic Press: New York, 1976; Vol. 1.
(11) *Biological Magnetic Resonance*; Berliner, L. J., Reuben, J., Eds.; Plenum Press: New York, 1978.
(12) Jost, P.; Libertini, L. J.; Hebert, V. C.; Griffith, O. H. *J. Mol. Biol.* **1971**, *59*, 77.
(13) Hwang, J. S.; Mason, R. P.; Hwang, L. P.; Freed, J. H. *J. Phys. Chem.* **1975**, *79*, 489.
(14) Polnaszek, C. F.; Freed, J. H. *J. Phys. Chem.* **1975**, *79*, 2283.
(15) Freed, J. H. *ACS Symp. Ser.* **1976**, *1*.
(16) Liang, Z. C.; Freed, J. H. *J. Phys. Chem. B* **1999**, *103*, 6384.
(17) Liang, Z. C.; Lou, Y.; Freed, J. H.; Columbus, L.; Hubbell, W. L. *J. Phys. Chem. B* **2004**, *108*, 17649.
(18) Lou, Y.; Ge, M. T.; Freed, J. R. *J. Phys. Chem. B* **2001**, *105*, 11053.
(19) Chiang, Y.-W.; Shimoyama, Y.; Feigenson, G. W.; Freed, J. H. *Biophys. J.* **2004**, *87*, 2483.
(20) Moser, M.; Marsh, D.; Meier, P.; Wassmer, K. H.; Kothe, G. *Biophys. J.* **1989**, *55*, 111.
(21) Lange, A.; Marsh, D.; Wassmer, K. H.; Meier, P.; Kothe, G. *Biochemistry* **1985**, *24*, 4383.
(22) (a) Abragam, A. *The Principles of Nuclear Magnetism*; Clarendon Press: Oxford, U.K., 1961. (b) Abragam, A. *The Principles of Nuclear Magnetism*; Clarendon Press: Oxford, U.K., 1961; Chapter 5, p 139.
(23) Lipari, G.; Szabo, A. *J. Am. Chem. Soc.* **1982**, *104*, 4546.
(24) Schurr, J. M.; Babcock, H. P.; Fujimoto, B. S. *J. Magn. Reson., Ser. B* **1994**, *105*, 211.
(25) Redfield, A. G. The Theory of Relaxation Processes. In *Advances in Magnetic Resonance*; Waugh, J. S., Ed.; Academic Press: New York, 1965; Vol. 1, p 1.
(26) Nielsen, R. D.; Robinson, B. H. *J. Phys. Chem. A* **2004**, *108*, 1589.
(27) Edmonds, A. R. *Angular Momentum in Quantum Mechanics*; Princeton University Press: Princeton, NJ, 1985.
(28) Hubbard, P. S. *Phys. Rev. A* **1974**, *9*, 9.
(29) Levi, G.; Marsault, J. P.; Marsault-Herail, F.; McClung, R. E. D. *J. Chem. Phys.* **1980**, *73*, 2443.
(30) Hubbard, P. S. *Phys. Rev.* **1963**, *131*, 1155.
(31) Biedenharn, L. C.; Louck, J. D. *Angular Momentum in Quantum Physics: Theory and Application*; Addison-Wesley: Reading, MA, 1981; Vol. 8.
(32) Hubbard, P. S. *Phys. Rev. A* **1977**, *15*, 329.
(33) McClung, R. E. D. *J. Chem. Phys.* **1980**, *73*, 2435.
(34) Hubbard, P. S. *Phys. Rev. A* **1973**, *8*, 1429.
(35) *CRC Handbook of Chemistry and Physics*, 56th ed.; Weast, R. C., Ed.; CRC Press: Cleveland, OH, 1975.
(36) Torrey, H. C. *Phys. Rev.* **1953**, *92*, 962.
(37) Hunt, B. I.; Powles, J. G. *Proc. Phys. Soc., London* **1966**, *88*, 413.
(38) DeGennes, P.-G. *J. Phys. Chem. Solids* **1958**, *7*, 345.
(39) Subczynski, W. K.; Pasenkiewicz-Gierula, M.; McElhaney, R. N.; Hyde, J. S.; Kusumi, A. *Biochemistry* **2003**, *42*, 3939.
(40) Fajer, P.; Thomas, D. D.; Feix, J. B.; Hyde, J. S. *Biophys. J.* **1986**, *50*, 1195.
(41) Fajer, P.; Feix, J.; Hyde, J.; Thomas, D. *Biophys. J.* **1986**, *49*, A469.
(42) Kubo, R.; Tomita, K. *J. Phys. Soc. Jpn.* **1954**, *9*, 888.
(43) Schwartz, L. J.; Millhauser, G. L.; Freed, J. H. *Chem. Phys. Lett.* **1986**, *127*, 60.
(44) Robinson, B. H.; Mailer, C.; Reese, A. W. *J. Magn. Reson.* **1999**, *138*, 210.
(45) Robinson, B. H.; Mailer, C.; Reese, A. W. *J. Magn. Reson.* **1999**, *138*, 199.